



Orientation dependences of the Fe-Li solid-liquid interface properties: Atomistic simulations



Xianglai Gan^a, Shifang Xiao^b, Huiqiu Deng^b, Xiaofan Li^b, Wangyu Hu^{a, b, *}

^a College of Materials Science and Engineering, Hunan University, Changsha 410082, China

^b Department of Applied Physics, School of Physics and Electronics, Hunan University, Changsha 410082, China

ARTICLE INFO

Article history:

Received 11 January 2016

Received in revised form

7 June 2016

Accepted 21 June 2016

Available online 23 June 2016

Keywords:

Fe-Li solid-liquid interface

Layering

Surface relaxation

Lateral order

Diffusion

Penetration

ABSTRACT

The Fe(110)-Li and Fe(111)-Li solid-liquid interfaces are investigated using molecular dynamics simulations (MD), and the results are detailedly compared with each other as well as with our previous findings obtained from the Fe(001)-Li solid-liquid interface. Due to the different intrinsic surface properties of the Fe substrates, the interface properties show remarkable orientation dependences. As for the Fe substrates, the three Fe surfaces suffer different impacts from the liquid Li on their relaxation behavior. The fine-scale density profiles suggest that the liquid Li atoms near the Fe(110)-Li solid-liquid interface are dramatically layered along the interface normal and the layers' two-dimensional density maps indicate the layers present high degree of lateral order, which are very similar to the results acquired from the Fe(001)-Li solid-liquid interface. Interestingly, these phenomena observed in the Fe(110)-Li solid-liquid interface do not reproduce in the Fe(111)-Li solid-liquid interface, but some distinct Li layers are detected along the [110] direction at 500 K. In addition, the Li atoms near the Fe(111)-Li solid-liquid interface diffuse faster and invade into the Fe substrate easier than those near the other two interfaces. These orientation-dependent characteristics are well explained in terms of the different surface properties of the Fe substrates.

© 2016 Elsevier B.V. All rights reserved.

1. Introduction

Solid-liquid interfaces exist commonly in our life. According to the constituent materials we can divide them into two classes: homogeneous solid-liquid interfaces and heterogeneous solid-liquid interfaces, and the latter exist more widely. Solid-liquid interfaces play important roles in engineering ranging from solidification, melting, corrosion, to liquid metal embrittlement and so on [1–6]. Therefore they have attracted a longstanding interest from scientists and technologists, however we still know little about them for their intrinsic complexity and the limitation of experimental condition. Most of our understandings come from theory researching and computer simulation. Using MD Buta et al. [7] investigated the structure and dynamics of Si crystal-liquid interface, ordered clusters with average lifetimes of 16 ps were found in the melt adjacent to the (111) facet. Sun et al. [8] studied the kinetics of isothermal crystallization and melting for Ni, and the

kinetic coefficients of the (100), (110) and (111) interfaces were calculated and discussed. Recently, Asadi et al. [9] have systematically calculated the solid-liquid interface free energies of Cu, Ni and Al via the capillary fluctuation method, the results agree well with the experimental measurements. In contrast to homogeneous solid-liquid interface, it is thorny in simulating heterogeneous solid-liquid interface for the difficulty encountered in constructing reliable alloy potentials. Attributing to the development of alloy potential in these years, more and more work focus on heterogeneous solid-liquid interfaces and the acquired knowledge deepen our understanding about these interfaces. Yang et al. [10] and Palafox-Hernandez et al. [11] detailedly characterized the Al-Pb and Cu-Pb solid-liquid interface, respectively, by the density, potential energy, stress and diffusion constant profiles, as well as the two-dimensional Fourier analysis of the interfacial layers. Nam et al. [4] and Rajagopalan et al. [5] examined the liquid metal embrittlement of the Al-Ga system, and Nam's results agree well with both the dislocation-climb model and general trends gleaned from the experimental studies. Hashibon et al. [12] created interatomic potentials for Ta-Cu system and the dewetting phenomenon of liquid Cu on Ta substrate was observed in their simulation. Using these potentials Yang [13,14] et al. studied the Ta-Cu solid-liquid

* Corresponding author. College of Materials Science and Engineering, Hunan University, Changsha 410082, China.

E-mail address: wuyuhu@hnu.edu.cn (W. Hu).

interface and the Ta-Cu50Ta50 solid-glass interface. Very recently, Turlo et al. [3] simulated the dissolution process of solid Ni in liquid Al and a diffusion-limited dissolution model has been developed. In order to unveil the grain refining mechanism of Al with different refiners, the interfaces between refiners and liquid Al have been extensively investigated [15–19]. The findings have exposed different refining mechanisms of different refiners and the different refining abilities of different crystal planes.

Stainless steels and liquid Li are the structure material and neutron generator, respectively, of the International Fusion Materials Irradiation Facility (IFMIF) [20,21]. The compatibility between them is an important problem, which directly relates to the stability and lifetime of the IFMIF. Acquiring the interface information is helpful to learn about the compatibility between the constituent materials and to find methods to improve the compatibility. Lately, we have explored the Fe(001)-Li solid-liquid interface using MD, which is a simplified model of the stainless steel-liquid Li interface [22]. The results showed that the liquid Li atoms near the interface were layered, during the simulation duration few Li atoms invaded into the Fe substrate even at 1100 K, and also few Fe atoms dissolved in the liquid Li. Previous literature reported that the interface properties present apparent orientation dependences [10,11,13–18], which suggests that to obtain a full view of the interface properties of the Fe-Li solid-liquid interface further work should be done. In this work, the Fe(110)/(111)-Li solid-liquid interfaces are examined and the results are compared with each other as well as with our previous findings, what's more we have illuminated the underlying mechanism of the orientation dependence observed in the interface properties.

2. Models and methods

Potential is the cornerstone of MD, and the potential used in this work can be found in a recently published paper of us [22]. This potential accurately reproduces the formation enthalpy of Fe-Li solid solution calculated from Miedema theory in all range. As we all know, the bcc to fcc phase transition occurs in pure iron near 1200 K [23], thus it is necessary to study the stability of the bcc structure in the temperature range we are interested in. To that end, a Fe sample with bcc structure has been adequately relaxed in a wide temperature range with this potential, and the structure analysis result indicates more than 84% atoms still keep the bcc structure at 1100 K, which means the bcc structure is still more stable than the fcc structure up to 1100 K. All the simulations were performed using our modified MOLDY code with a timestep of 2 fs. In all simulations, the periodic boundary condition was imposed on all directions, the Parrinello-Rahman barostat [24] and Nose-Hoover thermostat [25,26] were applied to control pressure and temperature, respectively. The detailed sample preparation process can be found in Refs. [22], which now we review. Two Fe samples with model parameters listed in Table 1 were relaxed adequately with *NPT* ensemble at certain temperatures, and then liquid Li samples were constructed by melting solid Li samples (the model parameters are listed in Table 1) using the *NP_zAT* simulation. The *NP_zAT* simulation is a variant of *NPT*, in which the sample is only allowed to relax along the *z* direction and the lengths of the other two dimensions are fixed to match the values of the Fe sample

obtained at the same temperature. The initial configurations of the Fe(110)/(111)-Li solid-liquid interfaces are constructed by conjoining the corresponding Fe and Li samples along the *z* axis. To ease the strong interactions between the close atoms, a 0.3 nm gap was inserted between the Fe and Li blocks. The initial configurations were relaxed 1.0 ns with *NP_zAT* simulation and then equilibrated under *NVT* ensemble to calculate the quantities we are interested in except the Li penetration depth. The initial configuration of the Fe(111)-Li solid-liquid interface was only relaxed 20 ps and then simulated with *NVT* to calculate the Li penetration depth.

3. Results and discussions

Generally speaking, interface properties can be reflected by the distributions of some physical quantities along the interface normal. Fine-scale density profile is defined as the statistical atom number density distribution (of a specific atom type or for all), for more details refer to [22]. In order to calculate this quantity, the samples adequately relaxed with *NP_zAT* simulation were sliced into many thin bins with sizes of 6.4×10^{-3} nm along the interface normal (*z* axis), and then the samples were relaxed with *NVT* ensemble to compute each bins' statistical atom number density of every atom type. Figs. 1 and 2 shows the temperature dependent fine-scale density profiles of the Fe(110)-Li and Fe(111)-Li solid-liquid interface, respectively (hereafter the Fe(001), (110) and (111)-Li solid-liquid interfaces are abbreviated as (001), (110) and (111) interfaces, respectively). It is clearly to see for the periodic arrangement of the crystal planes the Fe fine-scale density profiles oscillate periodically in these two cases. While for the narrower spacing between two neighboring (111) crystal planes the density peaks in the (111) interface are much denser. Temperature effect results in some interesting differences. For the (110) interface, the temperature increase caused intensification of atom vibration leads to the decrease of the peak values; but for the (111) interface besides the decrease of the peak values two interesting things are observed. First, contrary to the density peaks, the density valleys climb up gradually for the intensified atom vibration and the narrow spacings between neighboring crystal planes. In addition, the density near the interface declines rapidly and the peaks become indistinct, which is attributed to the low stability of the Fe atoms near the interface and we will further discuss in the following. In order to investigate the relaxation behavior of the Fe crystal planes near the surface before and after contacting with liquid Li, the interlayer spacings (defined as the distance between two neighbor density peaks, and in this case the sizes of the bins used to calculate the fine-scale density are set to be 1/2000th of the lattice constant of Fe at the corresponding temperature) between the first 16 crystal planes have been calculated and shown in Figs. 3 and 4. As the results show, in the three cases (the results of Fe(001) not show here) surface relaxation only occurs in the first three to four crystal planes and then the interlayer spacing converges to the bulk value although a certain degree of fluctuation presented for the relative high temperature. Furthermore, a larger fluctuation is observed in the bulk Fe before contacting with liquid Li. More interestingly, the fluctuation increases slightly with temperature for the clean Fe(001) and Fe(110) surfaces, while it is reversed for the Fe(111) surface. For the Fe(110) surface, the liquid Li just slightly changes

Table 1

The model parameters of the initial Fe(110) and Fe(111) samples as well as the parameters of the solid Li sample used to prepare the liquid Li samples.

	x	y	z	x length (Å)	y length (Å)	z length (Å)	Atom number
Fe(110)	1 $\bar{1}$ 0	00 $\bar{1}$	110	44.50	45.77	72.82	12,672
Fe(111)	1 $\bar{1}$ 0	11 $\bar{2}$	111	40.45	42.04	74.32	10,800
Li	100	010	001	41.80	41.80	104.49	8640

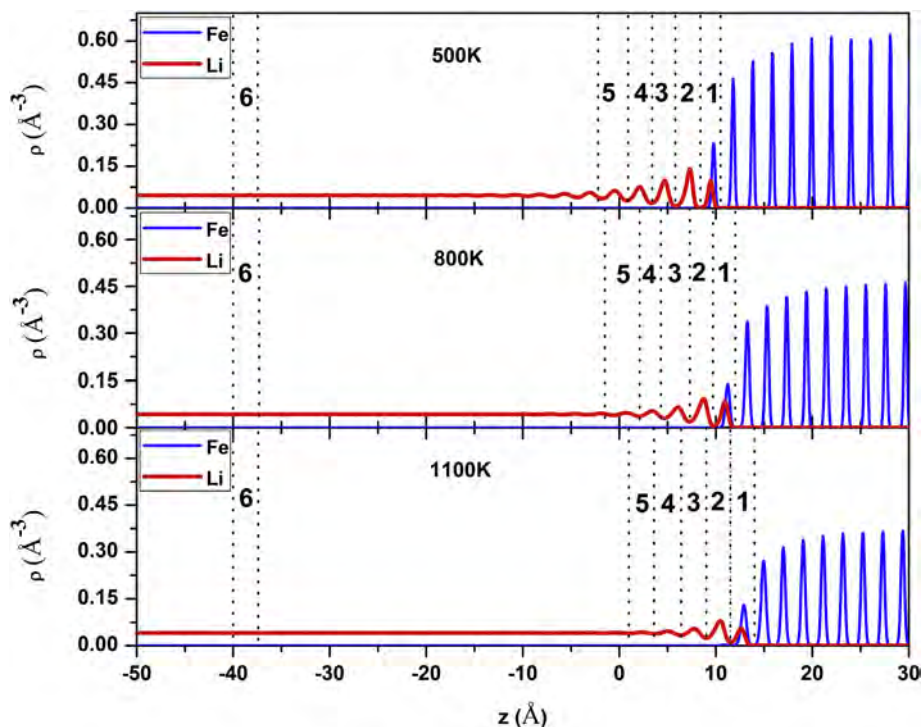


Fig. 1. The fine-scale density profiles of the Fe(110)-Li solid-liquid interface at 500 K, 800 K and 1100 K.

the relaxation behavior of the crystal planes near the surface, and the first two crystal planes are basically under contraction state whether contacting or not contacting with liquid Li. Although the first several crystal planes present remarkable temperature-dependent relaxation behavior on the clean Fe(111) surface, they are all under contraction state after contacting with liquid Li. As for

the Fe(001) surface, the result is totally different. Specifically, the first layer contracts (except at 1100 K) and the second layer expands on the clean surface; however, after contacting with liquid Li, the first layer transforms from contraction to expansion but the second layer recovers to the bulk value. It is worth to note that some discrepancy exists in Refs. [27–29] (and the references therein)

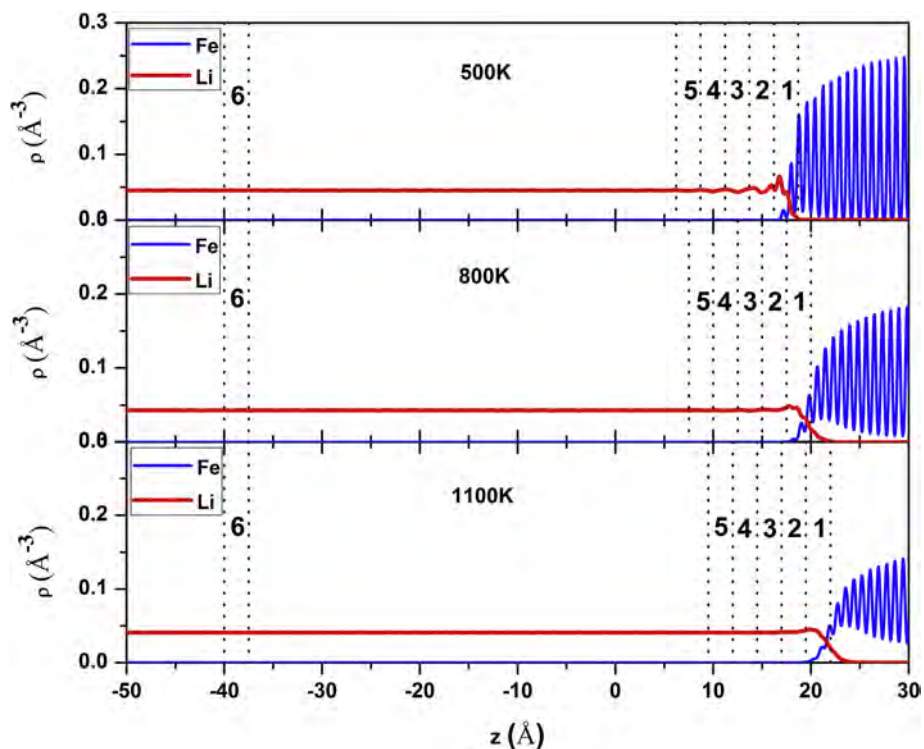


Fig. 2. The fine-scale density profiles of the Fe(111)-Li solid-liquid interface at 500 K, 800 K and 1100 K.

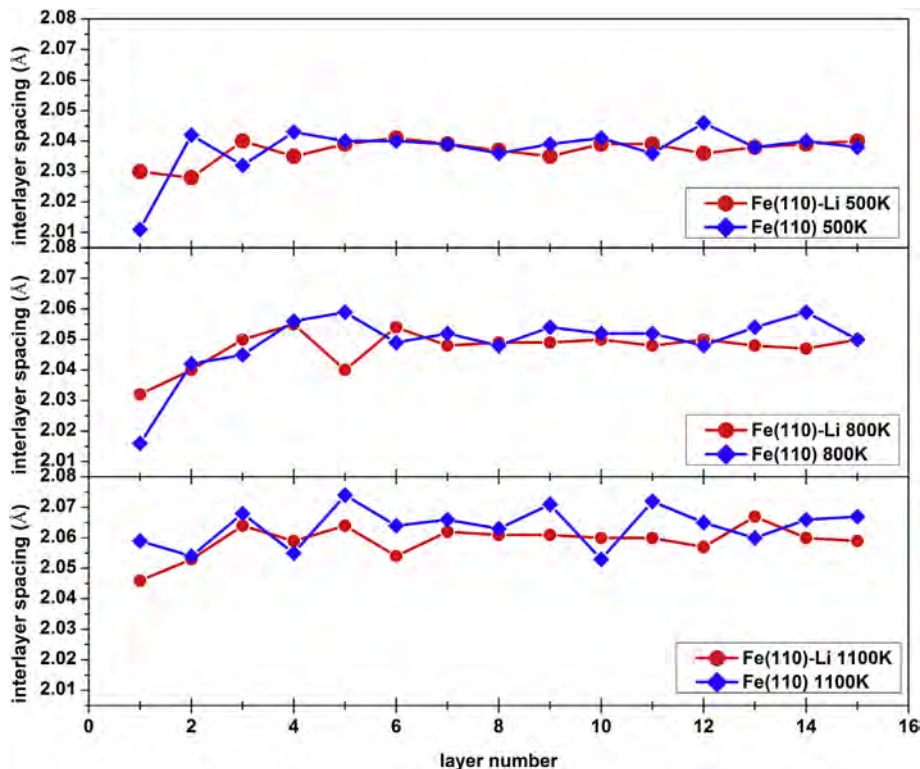


Fig. 3. The temperature-dependent interlayer spacing of the Fe(110) surface and the Fe(110)-Li solid-liquid interface.

about the relaxation behavior of the clean Fe surfaces. Our results basically agree with Błoński's results qualitatively [28,29], and the difference may be caused by the different temperatures we focused on. Unfortunately, no reference values can be used to compare with

for the interface cases. Much more attention should be focused on the Li fine-scale density profiles. In the (110) interface, the Li fine-scale density profiles present dramatically oscillation near the interface especially at 500 K, which is a signal of layering of the

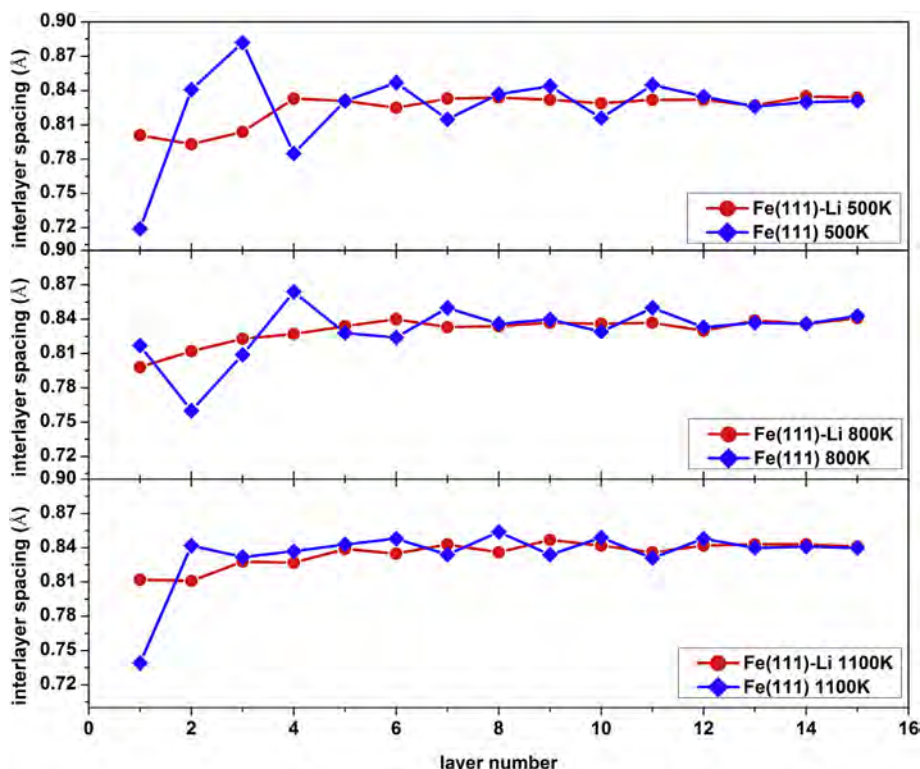


Fig. 4. The temperature-dependent interlayer spacing of the Fe(111) surface and the Fe(111)-Li solid-liquid interface.

liquid Li atoms adjacent to the interface. As temperature increasing, the density peaks decrease gradually and some peaks far from the interface even disappear. These findings are very similar to the results obtained from the (001) interface [22]. It is worth mentioning that as observed in the (001) interface the Li peak nearest to the interface overlaps the Fe peak nearest to the interface (show in Fig. 1), which means some Fe atoms in that Fe crystal plane are replaced by Li atoms. To our surprise, significant differences emerge in the results of the (111) interface. On one hand no clear visible density peaks are detected except some small ones at 500 K, on the other hand a wide density overlapping range appears near the interface at temperatures above 500 K. Obviously, the wide density overlapping range indicates some Li atoms invaded into the Fe block. The aforementioned characteristics can be further confirmed by the interface snapshots displayed in Fig. 5. The first column presents the (110) interfaces saw from the $[1\bar{1}0]$ direction at different temperatures; the second and third column shows the (111) interfaces saw from the $[11\bar{2}]$ and $[1\bar{1}0]$ direction, respectively. As the fine-scale density profiles suggested several distinct Li layers paralleling the interface are observed near the (110) interface at 500 K, as temperature increasing the layers far from the interface become blurry even disappear. Such landscape does not reproduce in the (111) interfaces. As we expected, however, the interface is much rougher than the (110) interface and a certain number of Li atoms invaded into the Fe substrates especially at high temperatures, which are different from the findings obtained from the other two interfaces. More interestingly some inclined Li layers are detected along the $[110]$ direction when seeing from the $[1\bar{1}0]$ direction at 500 K. These interesting phenomena will be further explained in the following.

Interface width is another critical index used to characterize an interface. To obtain this quantity, the coarse-grained density profile should be calculated first. The coarse-grained density of a specific bin mentioned above is equal to a weight averaged value of its and its neighboring bins' total fine-scale density and the detailed computation procedure is described in Ref. [7]. The coarse-grained

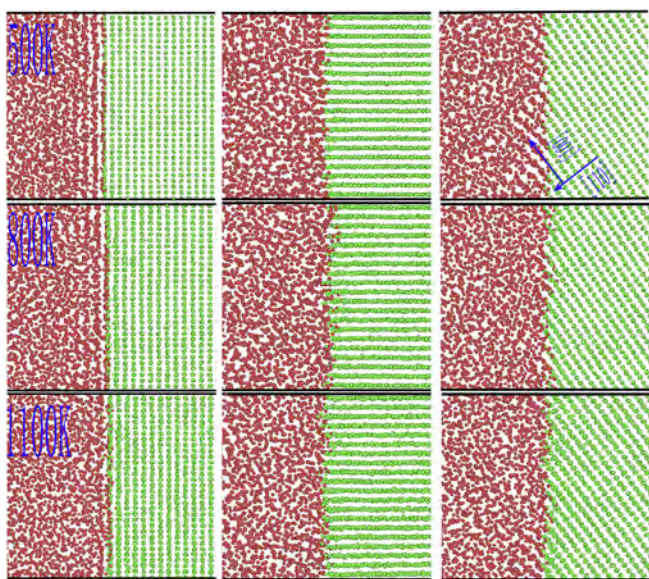


Fig. 5. The snapshots of the Fe(110)/(111)-Li solid-liquid interface. The first to third row represents the interfaces at 500 K, 800 K and 1100 K, respectively. The first column represents the Fe(110)-Li solid-liquid interface saw from the $[1\bar{1}0]$ direction, the second and third column represents the Fe(111)-Li solid-liquid interface saw from the $[11\bar{2}]$ and $[1\bar{1}0]$ direction, respectively. The red dots represent Li atoms and the green dots represent Fe atoms. (For interpretation of the references to colour in this figure legend, the reader is referred to the web version of this article.)

density profiles of the (110) and (111) interfaces together with their fitting curves are displayed in Fig. 6. As in our previous study [22] a hyperbolic tangent function $f(z) = c_1 + c_2 \tanh [c_3(z - c_4)]$ is utilized in fitting, where c_1 , c_2 , c_3 and c_4 are the fitting parameters. It is obvious that the fitting curves match well with the coarse-grained density profiles, and the values in bulk liquid Li and solid Fe are two invariant constants (f_l and f_s) which are connected smoothly in a narrow interface region. The finite-width of the transition regions indicate the interfaces are not ideal planes, as in our previous work [22] the range between $f_l + 10\%(f_s - f_l)$ and $f_s - 10\%(f_s - f_l)$ is defined as the interface width which is labeled in Fig. 6. The temperature dependent interface widths for the (110) and (111) interfaces are depicted in Fig. 7. It clearly shows that in these two cases the interface width increases linearly as temperature rises, and the fitting formulas for the (110) and (111) interfaces are $y = 8.1724 + 7.9475 \times 10^{-4} T$ and $y = 8.0550 + 1.19 \times 10^{-3} T$, respectively. Interestingly, the interface width increases exponentially with temperature in the (001) interface [22], which is significant different from the results obtained here.

A comparative analysis of the structure and diffusion property of the liquid Li atoms near these interfaces is helpful to construct a full view of the interface properties, which is carried out within the six atom layers labeled in Figs. 1 and 2. Different standards are adopted in ascertaining these layers from the fine-scale density profiles for the (110) and (111) interface. For the (110) interface, the first five atom layers' (layer 1 to layer 5) boundaries are determined by the two neighboring troughs of the corresponding density peaks, and the sixth layer locates in the bulk liquid Li with a size equating to the average of the first five layers' width. Since no density peaks are clearly observed in the Li fine-scale density profiles of the (111) interface, the method utilized in the (110) interface is inoperable. In this case all layers' widths are set to 0.25 nm, which is equal to the average of the first five layers' widths obtained from the (110) interface at 500 K. Two-dimensional density map [22] is an intuitive and appropriate quantity in characterizing the degree of lateral order of these layers. Here, the two-dimensional density maps of the first three layers are calculated for these two interfaces at 500 K and the results are showed in Figs. 8 and 9 respectively. For the (110) interface, as the layer 1 composed of Fe and Li atoms the two-dimensional density maps of these two types of atoms are calculated and exhibited in Fig. 8(a) and (b), respectively. Apparently, in this layer the Fe and Li atoms form immiscible small "islands" and the whole layer still maintains the structure of the (110) crystal plane. The next two layers also present the symmetry as we observed in the layer 1, however the degree of lateral order decreases gradually as the layer is far away from the interface. Similar features were discovered in the (001) interface except the layers presenting different symmetry and higher degree of the lateral order [22]. As we expected the (111) interface shows significant differences, in which the layer 1 and 2 show faintly visible symmetry of the Fe(111) crystal plane but present much lower degree of the lateral order than the corresponding ones in the (110) interface. In addition, there are two things worth noting. First, despite the layer 1 also constituted of Fe and Li atoms, these two types of atoms mix more uniformly (see Fig. 9(a) and (b)). Second, some approximately uniformly distributed high density small regions are still seen in the layer 2 (Fig. 9(c)), while the density map of the layer 3 is more uniform like a pierced spongia.

The diffusion constant profile, namely the diffusivity distribution along the interface normal, is frequently adopted to characterize the diffusion ability of the atoms locating in different layers [10,11,13,22]. However, after an in-depth analysis we find that it is difficult sometimes even impossible to obtain this quantity. To calculate the diffusivity of the atoms locating in a specific layer, the time-dependent mean square displacements (MSD) of the atoms

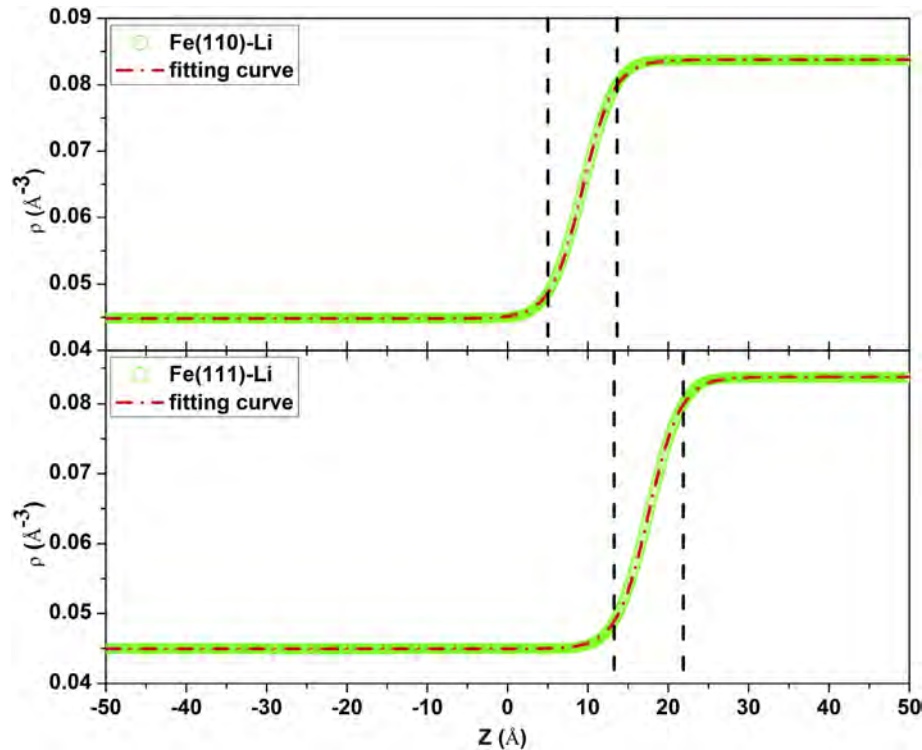


Fig. 6. The coarse-grained density profiles of the Fe(110)/(111)-Li solid-liquid interfaces together with their fitting curves at 500 K.

should be computed first and then the diffusivity is calculated according to the Einstein relation. It should be pointed out the MSD must be calculated in sufficient time, otherwise the Einstein relation does not hold. During that time, however, some atoms may run out of the layer for their high mobility and the narrow width of the layer, especially at high temperatures. Thus in that case this quantity becomes ambiguity and loses its meaning. Here another quantity, unleaving-atom ratio, is proposed to characterize the diffusion ability of the atoms along the interface normal. The unleaving-atom ratio of a specific layer is defined as the ratio between the number of atoms still inside the layer after a period of time and the initial total atom number of the same layer. The temperature- and time-dependent unleaving-atom ratios of the six

layers labeled in Figs. 1 and 2 are plotted in Figs. 10 and 11, respectively. Take the results of the (110) interface obtained at 500 K as an example. As time increasing all layers' unleaving-atom ratios decrease gradually but with different average decrease velocities. Specifically the layers far from the interface have larger average decrease velocities than the near ones, in other words the atoms in a layer far from the interface diffuse faster than those in a near one. This conclusion is in line with the finding obtained from the two-dimensional density maps. In addition, as the layer is gradually away from the interface its time-dependent unleaving-atom ratios converge to the values obtained from the bulk of liquid (layer 6) step by step. It is worth mentioning these conclusions agree with those acquired from the (001) interface despite the diffusion constant profile adopted in that case. Note that only after 38 ps more than 70% atoms run out of the layers 3 to 6, which strongly proves that it is more reasonable to use the unleaving-atom ratio to characterize the diffusion ability of the atoms in narrow layers. As temperature increasing the corresponding layers' values decrease gradually that means the higher the temperature the faster the diffusion. Similar characteristics are observed in the results of the (111) interface, but roughly speaking the atoms in the layers near the interface (about layer 1 to layer 3) diffuse faster than those in the corresponding layers of the (110) interface.

The fine-scale density profiles and the interface snapshots indicate that at high temperatures a certain amount of Li atoms invaded into the Fe substrate in the (111) interface, which is significantly different from the other two interfaces. In this case the penetration depth is calculated to characterize the penetration ability of the Li atoms, which is defined as the distance between the deepest Li atom and the interface, and the interface location is determined by the position of the deepest Li atom in the initial configuration. The temperature- and time-dependent penetration depths of the (111) interface are depicted in Fig. 12. It clearly shows that at 500 K the penetration depth always fluctuates around a low value 0.5 Å, however as temperature increasing the penetration

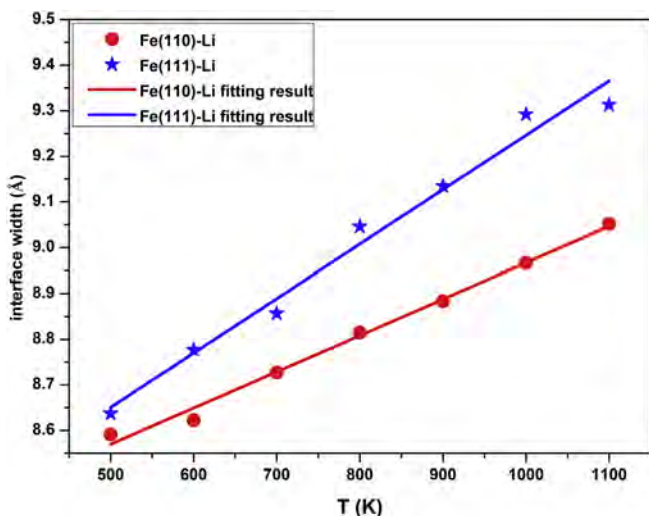


Fig. 7. The temperature-dependent interface widths as well as their fitting curves for the Fe(110)/(111)-Li solid-liquid interfaces.

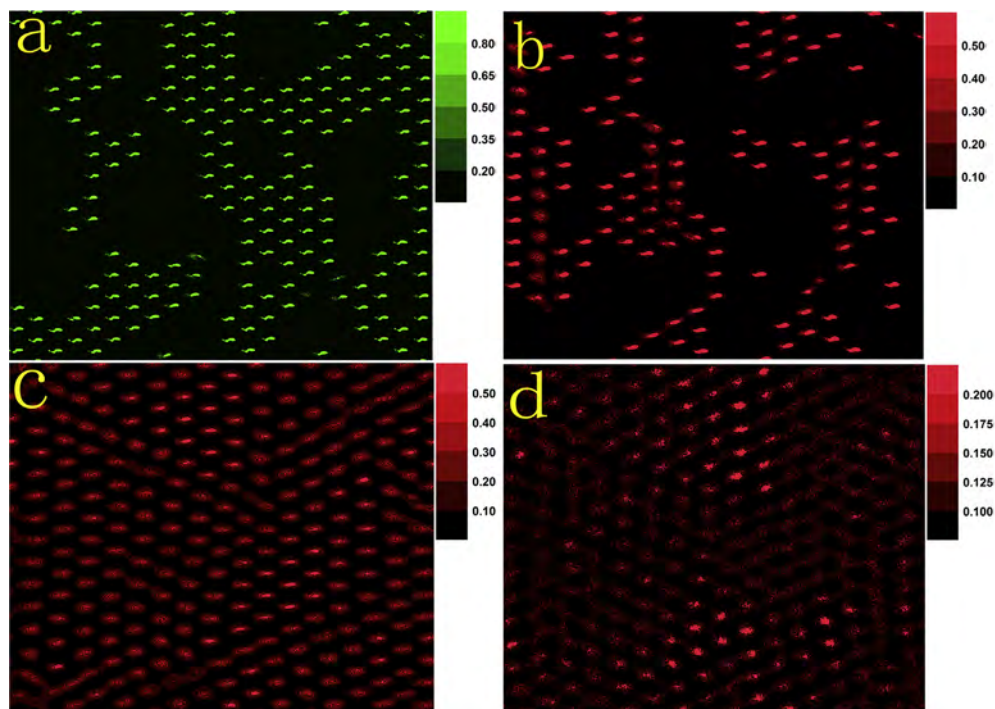


Fig. 8. The two-dimensional density maps for the first three layers of the Fe(110)-Li solid-liquid interface at 500 K: (a and b) the two-dimensional density maps for Fe and Li atoms in layer 1, respectively; (c and d) for Li atoms in layer 2 and 3, respectively (almost no Fe atoms in these two layers). The first three interfacial layers are illustrated in the fine-scale density profiles at 500 K.

depth increases gradually and the value reaches about 4.5 Å at 1100 K after 2.0 ns. Although this value is still small, it means the Li atoms traversed five (111) crystal planes. And considering such a short time this penetration depth is really considerable. The easier penetration property of the Fe(111) substrate is originated from the

lower stability of the Fe atoms on the (111) surface, which will be discussed in the following.

Now let's uncover the underlying mechanism regarding the aforementioned orientation dependences of the interface properties. Obviously the orientation dependences should attribute to the

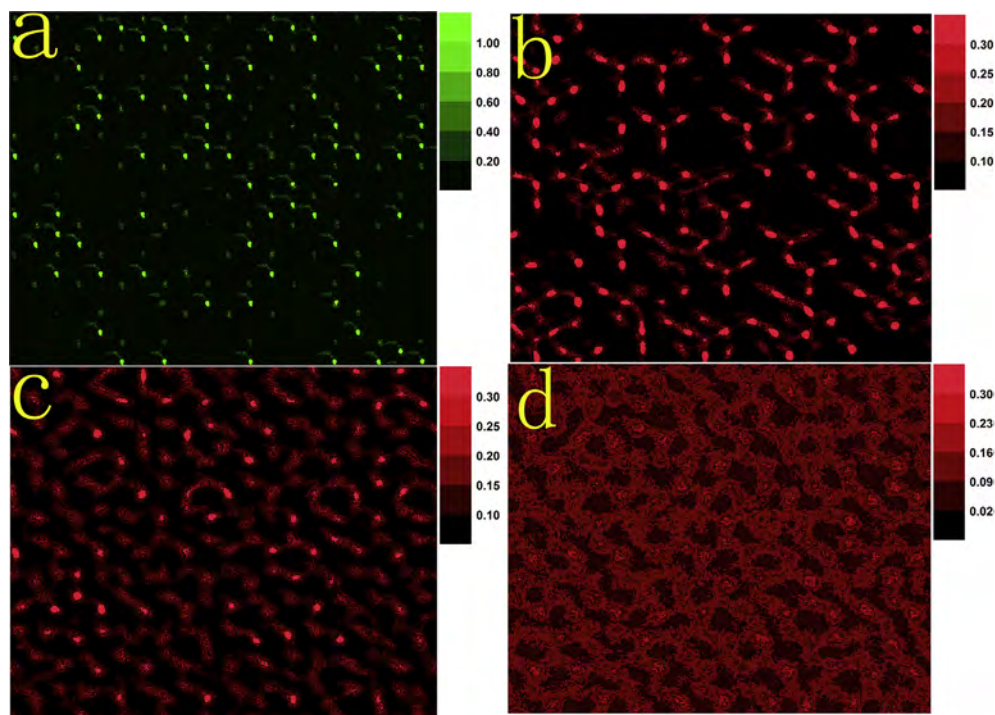


Fig. 9. The two-dimensional density maps for the first three layers of the Fe(111)-Li solid-liquid interface at 500 K: (a and b) the two-dimensional density maps for Fe and Li atoms in layer 1, respectively; (c and d) for Li atoms in layer 2 and 3, respectively (almost no Fe atoms in these two layers). The first three interfacial layers are illustrated in the fine-scale density profiles at 500 K.

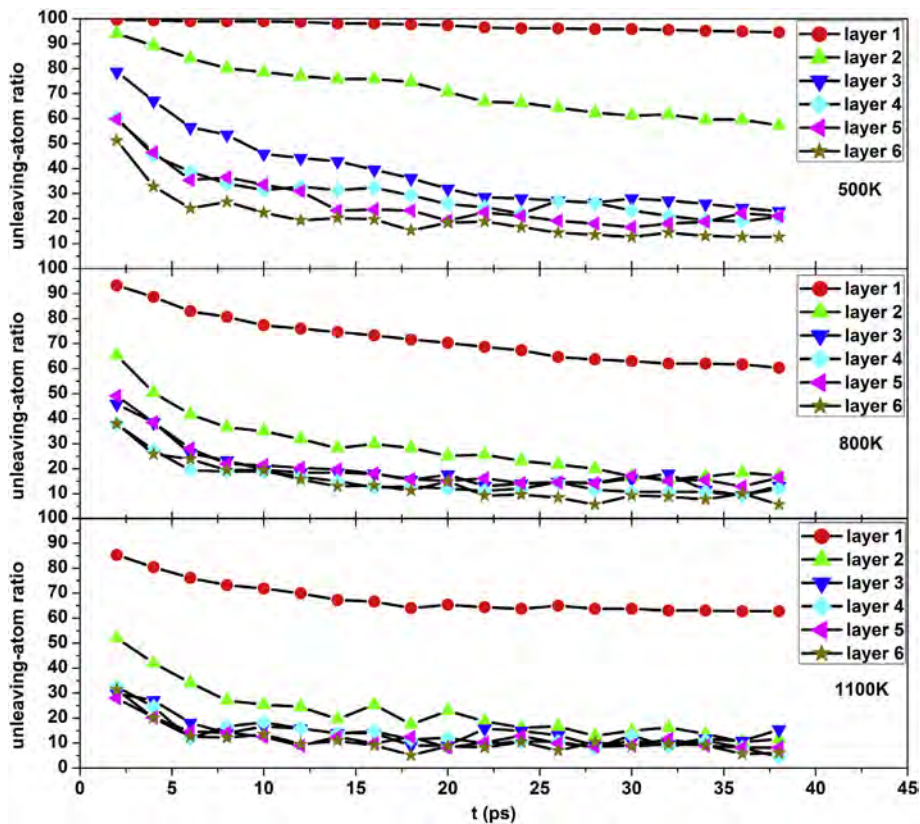


Fig. 10. The temperature- and time-dependent unleaving-atom ratio of the atoms located in the six layers labeled in Fig. 1.

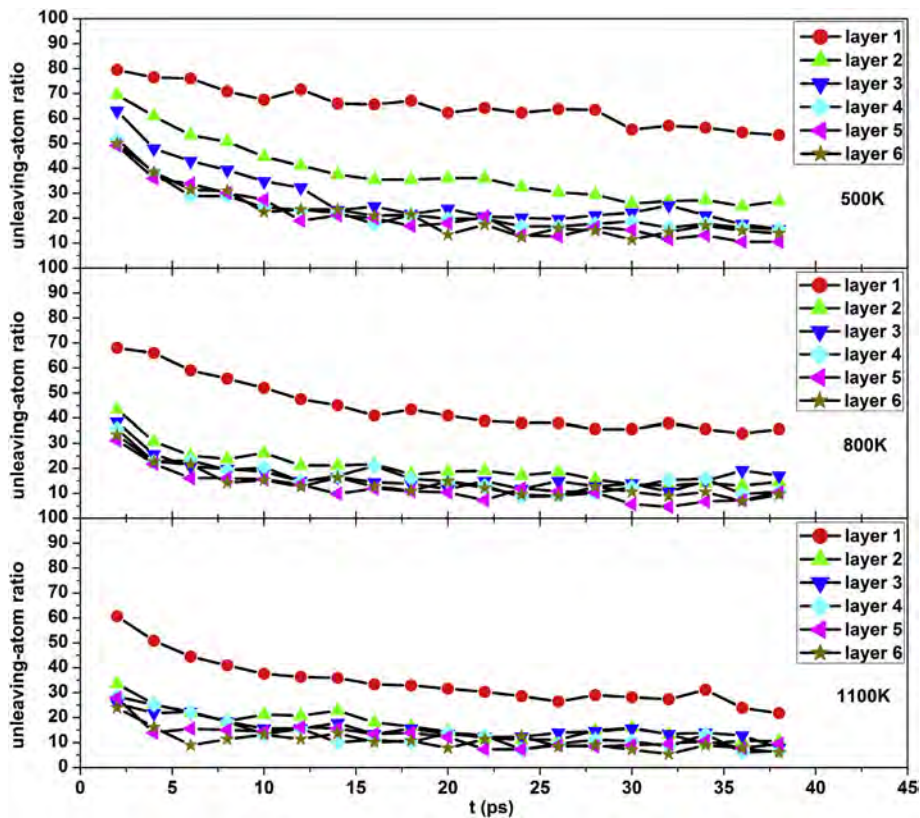


Fig. 11. The temperature- and time-dependent unleaving-atom ratio of the atoms located in the six layers labeled in Fig. 2.

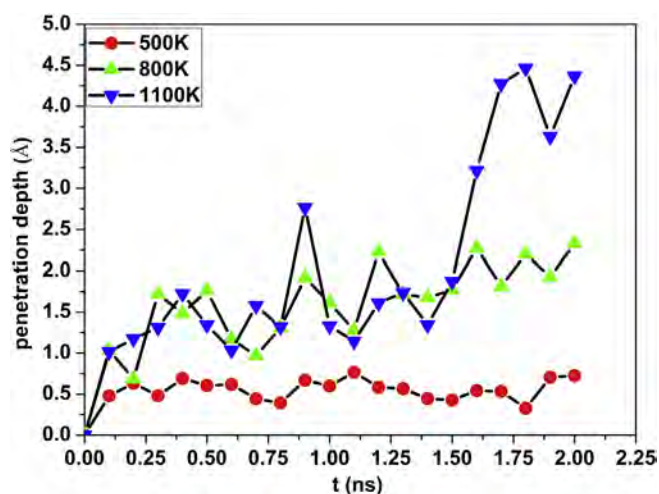


Fig. 12. The temperature- and time-dependent penetration depth of the Li atoms in the Fe(111)-Li solid-liquid interface.

different intrinsic surface properties of the Fe substrates terminated with different crystal planes. As we all know the liquid Li atoms near the interface suffer the influence from the potential field generated by the Fe substrate, at the same time interfacial Fe atoms suffer the collisions from the Li atoms as well. A stable potential field, with a number of regular and deep wells, is a prerequisite condition to induce the liquid Li atoms ordering. Apparently, a stable potential field is generated by a stable Fe substrate—more specifically the Fe atoms near the interface, so the stability of the Fe atoms near the interface is an important indicator that used to evaluate the ability of the Fe substrate in inducing the liquid Li atoms ordering. At the same time the stability is also an appropriate index applied to reflect the ability of the interfacial Fe atoms to withstand the collisions from the Li atoms. For simplification, the stability of the Fe atoms on the (001), (110) and (111) surfaces is used to estimate the stability of the Fe atoms in the corresponding interfaces. Residual bond number, escape energy and surface energy are three important quantities used to characterize the stability of the surface atoms. The escape energy of one Fe atom on different surfaces is defined as the energy difference of the system before and after the Fe atom pulled into vacuum enough far at 0 K. For the weak interactions between the farther apart atoms, in this work only the first and second neighbor bonds are taken into consideration when counting the residual bond number. The calculated residual bond numbers and escape energies of the atoms on the Fe(001), Fe(110) and Fe(111) surface are listed in Table 2. It shows that the (110) surface atoms have the most total bond number and first neighbor bond number, and the (001) surface atoms have the same number of first neighbor bond as the (111) surface atoms but have more second neighbor bond. These results indicate the (001) and (110) surface atoms are more stable than those on the (111) surface, which is further validated by the escape energies and consistent well with the result from Xu [30]. Fig. 13 shows the temperature-dependent surface energies of these three surfaces calculated with our potential together with the

Table 2

The first and second nearest neighbor bonds and escape energy of the Fe(001), Fe(110) and Fe(111) surface atoms calculated at 0 K.

	Fe(001)	Fe(110)	Fe(111)
First nearest neighbor bonds	4	6	4
Second nearest neighbor bonds	5	4	3
Escape energy (eV)	4.773	5.016	4.226

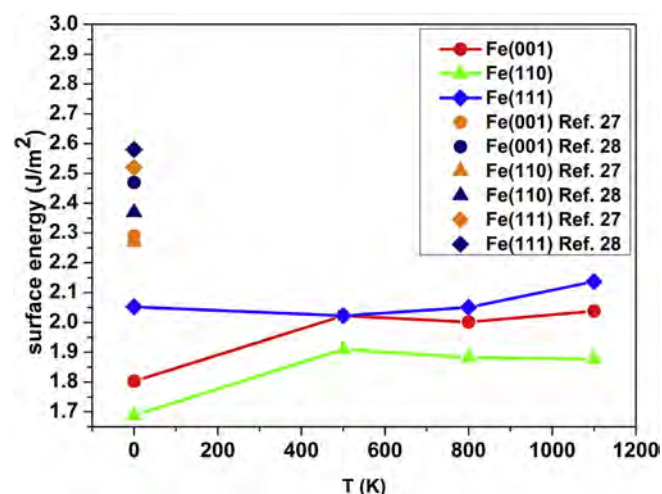


Fig. 13. The temperature-dependent surface energy of the clean Fe(001), Fe(110) and Fe(111) surfaces.

results obtained from density functional theory [27,28]. It is clear that the surface energy varies slightly as temperature increases in the three cases, and the results indicate the Fe(001) and Fe(110) surfaces are always more stable than the Fe(111) surface, which agrees well with the conclusion derived from the escape energies and the results of density functional theory although our results are smaller than the reference values. It is particularly worth mentioning that the stability order obtained here is consistent with that obtained from experiment at 970 K [31]. Now we can doubtless say that the Fe(001) and Fe(110) surfaces are more stable than the Fe(111) surface at the temperatures adopted in this work. On the basis of the above analysis we know that the more stable the Fe atoms near the interface the more ordered the Li atoms near the interface, and that's why the Li atoms near the (001) and (110) interfaces are more ordered than those near the (111) interface. As we observed in the two-dimensional density maps the Li atoms near the (111) interface pack in the form of the (111) crystal plane, however for the narrow spacing between two neighboring (111) crystal planes and the lower degree of the lateral order of these Li(111) crystal planes no layering was clearly observed in the fine-scale density profiles and in the snapshots. On the contrary, for the larger spacing between two neighboring (110) crystal planes some ordered Li layers are observed clearly in the (111) interface along the [110] direction at 500 K. As temperature increasing, these Li layers disappear more quickly than those observed in the other two cases for the lower stability of the Fe atoms near the (111) interface. The higher the degree of order of the atoms, the slower their diffusion, hence it reasonably explains why the atoms near the (110) interface diffuse slower than those adjacent to the (111) interface at the same temperature. The lower stability of the (111) surface atoms also leads to the Li atoms invade into the Fe(111) substrate easier, therefore a certain amount of Li atoms penetrated in the Fe(111) substrate. This finding implies that strengthening the stability of the interfacial Fe atoms can improve the compatibility between the liquid Li and the stainless steels.

4. Conclusions

In summary, the Fe(110)-Li and Fe(111)-Li solid-liquid interfaces were investigated with MD, and the results were compared with each other as well as with our previous findings from the Fe(001)-Li solid-liquid interface. The interface properties exhibit significant orientation dependences. Although the three Fe surfaces all relaxed

within three to four crystal planes whether contacting or not contacting with liquid Li, they suffered different impacts from the liquid Li on their relaxation behavior. The Fe(001) surface almost totally reversed the relaxation behavior after contacting with the liquid Li, on the contrary just a very small change was observed in the Fe(110) case. For the similar intrinsic properties, the higher stability of the surface atoms, of the Fe(001) and Fe(110) substrates, the liquid side present similar characteristics in the Fe(001)-Li and Fe(110)-Li solid-liquid interfaces. In these two cases, the liquid Li atoms near the interface are layered and the layers present high degree of lateral order with symmetries of the (001) and (110) crystal planes, respectively. While for the very narrow spacing between two Li(111) crystal planes, no apparent layering was observed in the liquid Li near the Fe(111)-Li solid-liquid interface when see from the $[11\bar{2}]$ direction. In addition, because of the lower stability of the Fe atoms near the (111) interface, the Li layers near the (111) interface present much lower lateral order degree than those in the other two cases. And also for the same reason the Li atoms near the (111) interface diffuse faster and invade into the Fe substrate easier than those near the (110) interface, which suggests that strengthening the stability of the surface atoms of the stainless steels is helpful to improve the compatibility between the liquid Li and stainless steels.

Acknowledgements

This work is supported by the Chinese National Fusion Project for ITER with Grant No. 2013GB114001 and National Natural Science Foundation of China with Grant Nos. of NSFC 51271075, NSFC-NSAF11076012 and NSFC 11472273.

References

- [1] Y. Mishin, M. Asta, Ju Li, *Acta Mater* 58 (2010) 1117–1151.
- [2] Wayne D. Kaplan, Yaron Kauffmann, *Annu. Rev. Mater. Res.* 36 (2006) 1–48.
- [3] V. Turlo, O. Politano, F. Baras, *Acta Mater* 99 (2015) 363–372.
- [4] Ho-Seok Nam, David J. Srolovitz, *Acta Mater* 57 (2009) 1546–1553.
- [5] M. Rajagopalan, M.A. Bhatia, M.A. Tschopp, D.J. Srolovitz, K.N. Solanki, *Acta Mater* 73 (2014) 312–325.
- [6] E. Pereiro-López, W. Ludwig, D. Bellet, *Acta Mater* 52 (2004) 321–332.
- [7] Dorel Buta, Mark Asta, Jeffrey J. Hoyt, *Phys. Rev. E* 78 (2008) 031605.
- [8] D.Y. Sun, M. Asta, J.J. Hoyt, *Phys. Rev. B* 69 (2004) 024108.
- [9] Ebrahim Asadi, Mohsen Asle Zaeem, Sasan Nouranian, Michael I. Baskes, *Acta Mater* 86 (2015) 169–181.
- [10] Yang Yang, David L. Olmsted, Mark Asta, Brian B. Laird, *Acta Mater* 60 (2012) 4960–4971.
- [11] J. Pablo Palafox-Hernandez, Brian B. Laird, Mark Asta, *Acta Mater* 59 (2011) 3137–3144.
- [12] Adham Hashibon, Alexander Y. Lozovoi, Yuri Mishin, Christian Elsässer, Peter Gumbsch, *Phys. Rev. B* 77 (2008) 094131.
- [13] G.Q. Yang, J.F. Li, Q.W. Shi, L.T. Kong, *Comput. Mater. Sci.* 86 (2014) 64–72.
- [14] Guiqin Yang, Xiaozhe Gao, Jinfu Li, J. Lingti Kong, *Appl. Phys.* 117 (2015) 015303.
- [15] Junsheng Wang, Andrew Horsfield, Udo Schwingenschlögl, Peter D. Lee, *Phys. Rev. B* 82 (2010) 184203.
- [16] H.L. Zhang, Y.F. Han, Y.B. Dai, S.S. Lu, J. Wang, J. Zhang, D. Shu, B.D. Sun, *J. Alloys Compd.* 615 (2014) 863–867.
- [17] Junsheng Wang, Andrew Horsfield, Peter D. Lee, Peter Brommer, *Phys. Rev. B* 82 (2010) 144203.
- [18] Z. Fan, Y. Wang, Y. Zhang, T. Qin, X.R. Zhou, G.E. Thompson, T. Pennycook, T. Hashimoto, *Acta Mater* 84 (2015) 292–304.
- [19] H.L. Zhang, Y.F. Han, W. Zhou, Y.B. Dai, J. Wang, B.D. Sun, *Appl. Phys. Lett.* 106 (2015) 041606.
- [20] Hiroo Nakamura, et al., *Fusion Eng. Des.* 84 (2009) 252–258.
- [21] H. Nakamura, M. Takemura, M. Yamauchi, U. Fischer, M. Ida, S. Mori, T. Nishitani, S. Simakov, M. Sugimoto, *Fusion Eng. Des.* 75–79 (2005) 1169–1172.
- [22] Xianglai Gan, Shifang Xiao, Huiqiu Deng, Xuegui Sun, Xiaofan Li, Wangyu Hu, *Fusion Eng. Des.* 89 (2014) 2894–2901.
- [23] R. Boehler, M. Nicol, M.L. Johnson, Internally-heated diamond anvil cell: phase diagram and P-V-T of iron, *Geophys. Monogr. Ser.*, in: M.H. Manghnani, Y. Syono (Eds.), *High Pressure Research in Mineral Physics*, 39AGU, Washington, D.C., 1987, pp. 173–176.
- [24] M. Parrinello, A. Rahman, *Phys. Rev. Lett.* 45 (14) (1980) 1196–1199.
- [25] Shuichi Nosé, *J. Chem. Phys.* 81 (1984) 511–519.
- [26] William G. Hoover, *Phys. Rev. A* 31 (3) (1985) 1695–1697.
- [27] Michelle J.S. Spencer, Andrew Hung, Ian K. Snook, Irene Yarovsky, *Surf. Sci.* 513 (2002) 389–398.
- [28] P. Błoński, A. Kiejna, *Surf. Sci.* 601 (2007) 123–133.
- [29] P. Błoński, A. Kiejna, *Vacuum* 74 (2004) 179–183.
- [30] Yichun Xu, Chi Song, Yange Zhang, C.S. Liu, B.C. Pan, Zhiguang Wang, *Phys. Chem. Chem. Phys.* 16 (2014) 16837–16845.
- [31] H.E. Grenga, K. Kumar, *Surf. Sci.* 61 (1976) 283–290.